Article

Developmental Cell

How Actin Initiates the Motor Activity of Myosin

Graphical Abstract

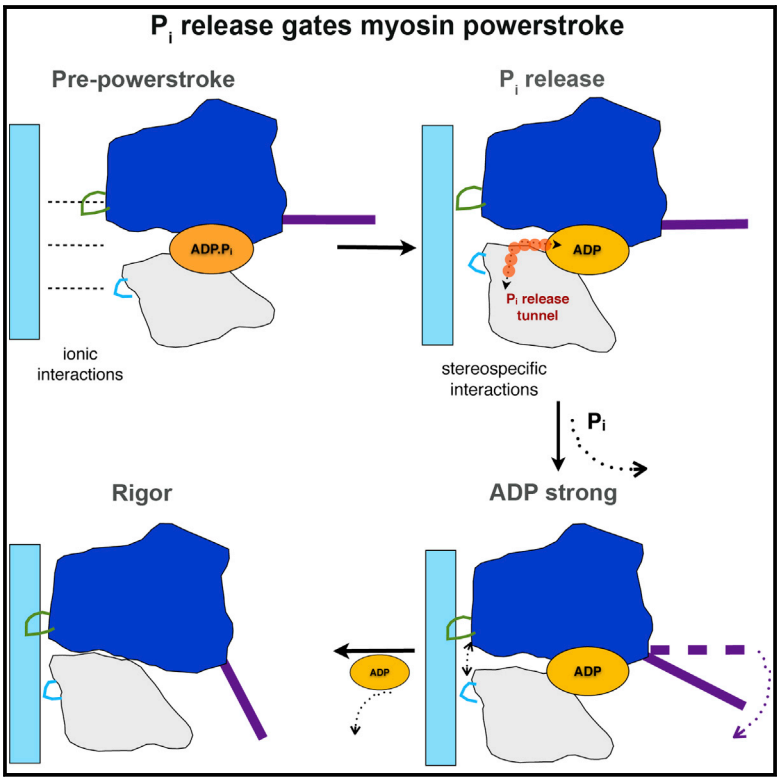

Highlights

- Myosin structure explains how actin binding initiates force generation
- P_i release from ATP hydrolysis precedes the major lever arm movement (powerstroke)
- P_i release pathway from ATPase and GTPase active sites may regulate their function

Authors

Paola Llinas, Tatiana Isabet, ...,
H. Lee Sweeney, Anne Houdusse

Correspondence

lsweeney@mail.med.upenn.edu (H.L.S.),
anne.houdusse@curie.fr (A.H.)

In Brief

Cellular tracks of microtubules and F-actin control the activity of molecular motors that interact with them. Llinas et al. combine structural and kinetic analyses to reveal that actin track binding activates myosin motors by opening an escape route for phosphate produced from ATP hydrolysis, triggering force generation and movement.

Accession Numbers

4PFO

Llinas et al., 2015, Developmental Cell *33*, 401–412
May 26, 2015
http://dx.doi.org/10.1016/j.devcel.2015.03.025

Developmental Cell
Article

How Actin Initiates the Motor Activity of Myosin

Paola Llinas,[1,2,4] Tatiana Isabet,[1,2,4] Lin Song,[3,4] Virginie Ropars,[1,2] Bin Zong,[3] Hannah Benisty,[1,2] Serena Sirigu,[1,2] Carl Morris,[3] Carlos Kikuti,[1,2] Dan Safer,[3] H. Lee Sweeney,[3,*] and Anne Houdusse[1,2,*]
[1]Structural Motility, Institut Curie, Centre de Recherche, Paris 75248, France
[2]CNRS, UMR144, 26 rue d'Ulm, Cedex 05, Paris 75248, France
[3]Department of Physiology, University of Pennsylvania School of Medicine, 3700 Hamilton Walk, Philadelphia, PA 19104-6085, USA
[4]Co-first author
*Correspondence: lsweeney@mail.med.upenn.edu (H.L.S.), anne.houdusse@curie.fr (A.H.)
http://dx.doi.org/10.1016/j.devcel.2015.03.025

SUMMARY

Fundamental to cellular processes are directional movements driven by molecular motors. A common theme for these and other molecular machines driven by ATP is that controlled release of hydrolysis products is essential for using the chemical energy efficiently. Mechanochemical transduction by myosin motors on actin is coupled to unknown structural changes that result in the sequential release of inorganic phosphate (P_i) and MgADP. We present here a myosin structure possessing an actin-binding interface and a tunnel (back door) that creates an escape route for P_i with a minimal rotation of the myosin lever arm that drives movements. We propose that this state represents the beginning of the powerstroke on actin and that P_i translocation from the nucleotide pocket triggered by actin binding initiates myosin force generation. This elucidates how actin initiates force generation and movement and may represent a strategy common to many molecular machines.

INTRODUCTION

Force production and force sensing in cells are of fundamental importance since mechanotransduction and directed movement are the basis of numerous cellular processes. Cytoskeleton motors interacting with cellular tracks play essential roles in such cellular functions as cell division, cell migration, intracellular trafficking, and proper formation and maintenance of the cell's specialized compartments (Hartman et al., 2011; Hirokawa et al., 2009; Roberts et al., 2013; Franker and Hoogenraad, 2013). Despite extensive investigations, how force and movement are produced by the sequential structural rearrangements of cytoskeleton motors triggered by interactions with their track remains unknown for microtubule-based motors (kinesins and dyneins) and actin-based motors that belong to the myosin superfamily. Currently, data are lacking that reveal how the sequential binding events of a molecular motor to its track can trigger force production. The critical initial track-binding event is linked to the release of inorganic phosphate (P_i) in the case of myosin and dynein molecular motors. In the case of kinesin motors, P_i release controls the end of the force-producing state. Thus, how the track controls phosphate release from these molecular motors is directly linked to the force production mechanism.

The myosin motor proteins power muscle contraction, as well as movement or force on actin filaments in all eukaryotic cells, via the cyclic interactions between myosin motors and actin filaments. Much progress has been made in understanding the changes in the myosin motor that lead to dissociation from actin by ATP and the subsequent conformational changes, known as the recovery stroke, that allow the hydrolysis of ATP. Following ATP hydrolysis, the myosin motor is in the pre-powerstroke (PPS) state and is primed for force production and movement on actin with MgADP and P_i trapped within the motor. Insights into the subsequent structural changes that actin promotes to generate force and movement are lacking (Sweeney and Houdusse, 2010), although there has been considerable speculation as to how this may occur (Geeves and Holmes, 2005; Gyimesi et al., 2008; Cecchini et al., 2010; Kull and Endow, 2013; Preller and Holmes, 2013). There is general agreement that the motor activity of myosin on actin is driven by actin's ability to catalyze the sequential releases of P_i and MgADP, which are coupled to conformational changes in the myosin motor that allow movement and force generation. What is commonly known as the myosin "head" contains all of the elements necessary for force generation and movement. Figure 1 describes the structural elements of the myosin motor. As also shown in Figure 1, the myosin head can be subdivided into a motor domain, which is the site of both actin-binding and ATPase activity, and the "lever arm," which consists of the C-terminal subdomain of the motor (converter) followed by an extended helix of variable length containing a number of consensus calmodulin or calmodulin-like light-chain binding sites. The myosin lever arm is followed by a coiled coil for two-headed myosin classes. Both single- and two-headed myosin classes contain C-terminal sequences that allow binding of the myosin to its cellular target(s)/cargo(s).

While the force generation mechanism is conserved, each motor has evolved to perform specific actions and to participate in multiple cellular processes. The rates of the force production transitions on the track and their force sensitivity differ among cytoskeleton motors to tune them for different cellular actions. Thus, structural and functional information on the motor mechanism is essential for investigating these differences and understanding the cellular processes in which multiple motors often work in synergy. From the standpoint of delineating the fundamental basis of chemo-mechanical transduction by myosin

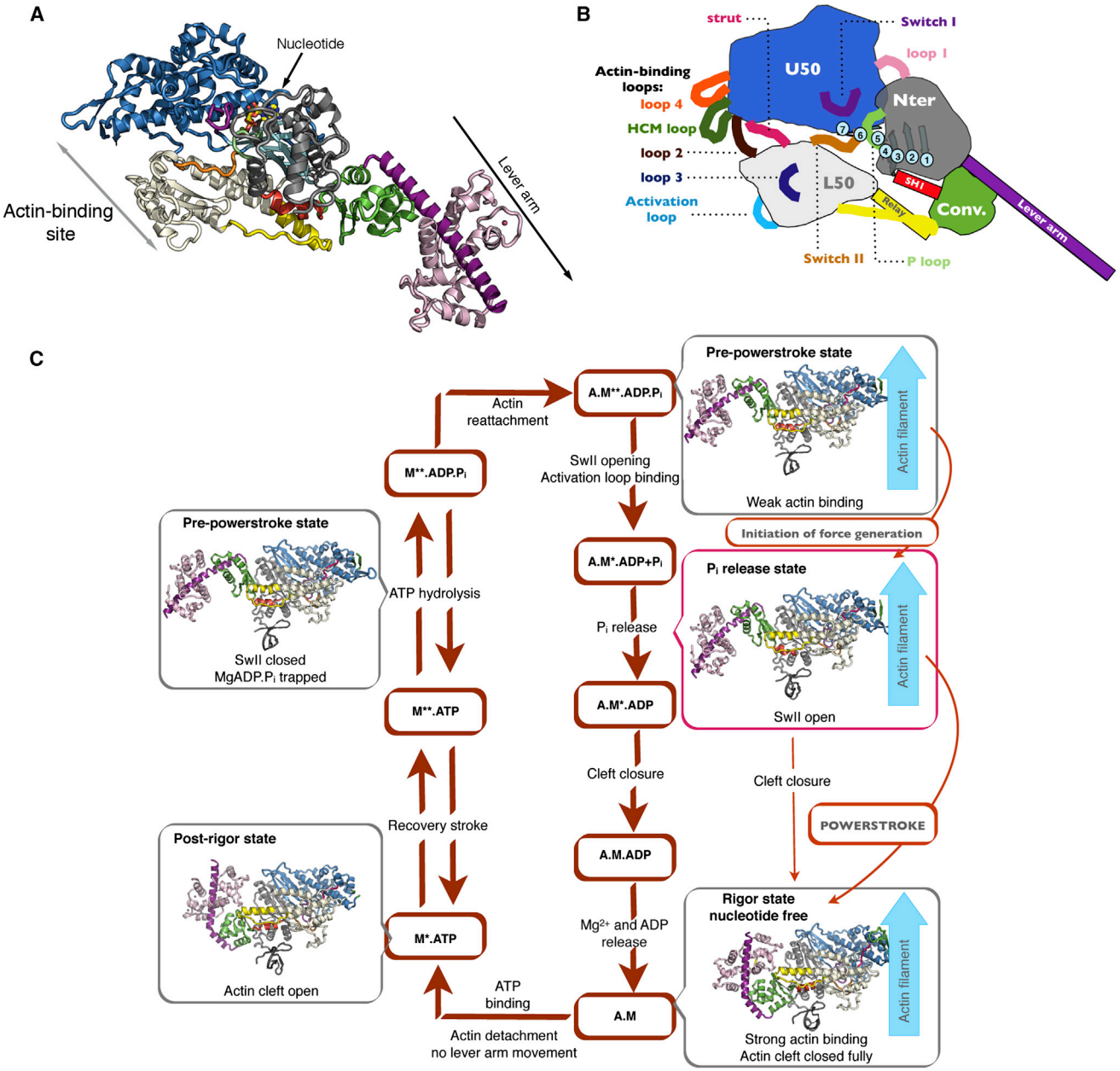

Figure 1. Actin-Myosin Force-Generating Cycle and Allosteric Rearrangements in Myosin Motors

(A) Ribbon diagram of the myosin VI motor domain in the P_i release state depicting the four subdomains: upper 50 (blue), L50 (white), N-ter (gray), and converter (green). The Insert 2 (violet) with a bound calmodulin (light pink) is an insertion that repositions the lever arm, acting as a reverse gear.

(B) Schematic representation of myosin VI showing important nucleotide-binding loops (switch I, switch II, P loop) and connectors (SH1 helix, relay helix, strut) as well as the five actin-binding loops [Loop2, HCM loop, Loop3, Loop4, and Activation loop]. The transducer (light blue) is a β sheet of seven strands belonging to the Nter and upper 50 (U50) subdomains. There is an important distortion in the transducer conformation between the Rigor state and the subsequent ATP-bound Post-Rigor and PPS states. Between the U50 and L50 subdomains, an internal cleft (so-called 50-kDa cleft) can form either near actin (outer cleft) or near the nucleotide (inner cleft defining the back door). Conv. converter.

(C) Actomyosin ATPase cycle showing the known structural states of myosin VI in the force-generating cycle. The motor domain of myosin VI is depicted in four structural states: Rigor (nucleotide-free, on F-actin), Post-Rigor (detached from F-actin, bound to an ATP analog), PPS (bound to ADP.P_i, representing post-hydrolysis with ADP.P_i trapped in the active site), and the P_i release state presented in this paper (bound to ADP+P_i or ADP, representing the state in which the P_i can be released). Note that the priming of the lever arm occurs upon the recovery stroke, prior to hydrolysis, when myosin is detached from actin. Quite different structural transitions within the myosin head trigger the powerstroke when myosin is bound on actin, and we propose that these are triggered after P_i release to produce directional movement on F-actin.

See also Figure S1.

motors, the actin-induced structural changes represent the most important area to investigate.

Myosin rapidly hydrolyzes ATP in the absence of actin, but rapid product release requires interaction with actin. Once phosphate and ADP have been released, ATP rapidly rebinds to the actin-bound myosin, causing rapid dissociation from actin. All forms of myosin have the same basic kinetic cycle (shown in Figure 1). In the absence of actin, P_i release is quite slow. Soon after the publication of the initial myosin structure (Rayment et al., 1993), it was noted that in order for actin-activated P_i release to precede ADP release, actin would likely create an escape route for phosphate that was an alternative to the normal exit to the nucleotide binding pocket (Yount et al., 1995). There has been much speculation as to the nature of the creation of the back door (Geeves and Holmes, 2005; Sweeney and Houdusse, 2010). What is clear is that in order for the phosphate to dissociate, actin binding must cause some rearrangement in either switch I or switch II (Figures 1B and S1). These elements, along with MgADP, block any possible dissociation of P_i. It is not obvious how either element can be induced to move by actin binding. The majority of investigators in the field favor a mechanism in which switch I is pulled away in order to create a phosphate escape route, which is denoted as the side door in Figure S1 (Geeves and Holmes, 2005; Gyimesi et al., 2008; Cecchini et al., 2010; Kull and Endow, 2013).

The appeal of switch I movement creating the exit site is largely based on the bias that switch II rearrangements must be coupled to lever arm movements, as in the recovery stroke transition (Geeves and Holmes, 2005). However, in order to allow the maximal possible movement and force generation on actin to occur, either no or minimal lever arm movement should occur until after myosin has bound strongly to actin. Thus, models have been proposed in which cleft closure would allow most interactions seen in Rigor to form in the beginning of the powerstroke state, so that myosin with a lever arm in the pre-stroke position would bind strongly prior to either P_i release or lever arm movement (Preller and Holmes, 2013). However, no data exist that suggest that cleft closure can promote an opening of the active site to allow P_i release. A major movement of switch I would result in loss of MgADP as well as P_i, leading to a myosin state that MgATP can rapidly detach from actin. Since myosin with MgADP bound is the primary force-bearing/generating state on actin, this would greatly limit force generation.

Herein, we present evidence that there is not formation of the Rigor-like actin interface prior to P_i release, in sharp contrast to prevailing models (Geeves and Holmes, 2005; Gyimesi et al., 2008; Cecchini et al., 2010; Kull and Endow, 2013; Preller and Holmes, 2013). We show that the major cleft closure at the actin interface follows P_i release. We present a structure that, we propose, represents the state that actin stabilizes for the initial release of P_i. In this P_i release state, the lever arm is in its ''primed'' or pre-stroke position, and the escape route for P_i release is created by a movement of switch II, with no movement of switch I. We assess whether this state indeed represents the P_i release state for myosin classes in general by creating a number of mutations and performing kinetic experiments in parallel on class VI, V, and II myosins.

These data demonstrate that the initial binding to the track (actin, in the case of myosin) induces a tunnel that allows phosphate to translocate away from the active site and exit the protein by first promoting a different type of structural change at the interface with the track, as compared to the conformational change that must follow in order to drive the lever arm swing (powerstroke). The importance of gating of the force-producing states by the track and the role of controlled sequential release of ATPase products to couple ATP usage to force production, as we report for myosin, elucidates what may be a general strategy for ATP-powered cellular machines; namely, that the effector protein induces a conformation that displaces the trapped phosphate from the active site, allowing the mechanical transitions to proceed.

RESULTS

A Structural State of Myosin with an Open Phosphate Escape Route

To create a back door for P_i release, there are only two options. Either switch I can rearrange in such a way as to maintain coordination of MgADP and yet create an escape route for phosphate, or switch II must rearrange to create the opening without a major change in the position of the lever arm (Figure S1). A series of crystallization experiments with fragments of myosin VI bound to MgADP yielded a previously unseen structural state that has unexpected attributes and could possibly be the missing P_i release structure (Figure 1A; Figure 2). The structure was determined to 1.75 Å resolution (P_iR; Table S1). It was also obtained in two different crystal forms (Figure S2A; Table S1), thus demonstrating that it did not arise from crystal packing. The characteristics of this structural state include the lever arm remaining in a primed position and a new actin interface. The transducer is similar to that found in the PPS state, but movement of the lower 50 (L50) subdomain has opened the inner cleft near where the P_i is trapped in the active site in the PPS state. While the inner cleft has opened, the outer cleft near actin is more closed than in the PPS state.

An important feature of the structure is that switch II has moved by 4 Å compared to its position in the PPS structure (Figure 2), opening a possible escape route for P_i, while the switch I and the P loop positions are unchanged, as is the MgADP coordination (Movie S1). What this structure demonstrates is that a large switch II opening compared to the PPS state, linked to the formation of this actin interface, does not trigger a large change in the lever arm position. As described in the Supplemental Information, we obtained a closely related *Dictyostelium* myosin II (DdII) structure that also shows that a large switch II movement in myosins can occur without a significant lever arm swing (Figure S2B).

It is interesting that the outer cleft near F-actin is closed to a greater extent than in the PPS state, due to a movement of the L50 subdomain (Figure 3). However, this involves a different relative rotation of subdomains than what is necessary to form the Rigor state (Figure 3). Thus, this P_iR state presents a different actin interface as compared to the PPS state (Figure 3), which may be necessary to allow stereo-specific binding. While it has been proposed that actin binding would close this cleft, it has generally been assumed that cleft closure would occur as seen in Rigor-like structures (Preller and Holmes, 2013) and would be coupled to lever arm movement, thus preceding P_i

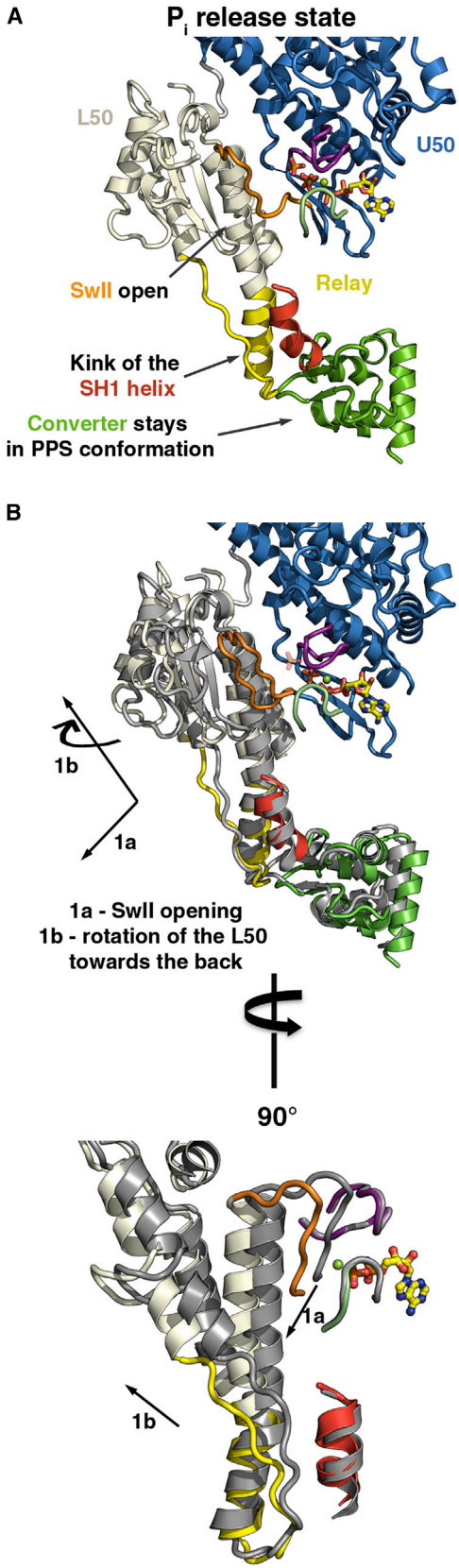

Figure 2. Features of the P_i Release Structure

(A) Hallmarks of the P_i release structure are highlighted in this figure. To open the phosphate-release route, switch II adopts a position that allows the converter to remain in its PPS conformation with a primed lever arm. This is, in part, made possible by a kink in the SH1 helix (red). The SH1 helix links the Nter subdomain (not shown for clarity) and the converter (green) and interacts with the relay helix and loop (yellow), thus playing a central role in the coordination of the movements between these subdomains. U50, upper 50.

(B) Comparison between the PPS (gray) and the P_i release (P_iR; color code as in Figure 1) myosin VI structures upon superimposition on their U50 and Nter subdomains. The black arrows (1a and 1b) indicate the movement of the L50 subdomain (white) and switch II (orange), necessary for the back door opening, giving rise to the P_iR structure. In the P_iR structure, there are no conformational changes in switch I (violet) or the P loop (lime) and limited change for the converter (green). A 90° rotation shows also these movements in more detail. See also Figure S2 and Table S1.

release (Geeves and Holmes, 2005; Muretta et al., 2013). As demonstrated later, the cleft closure sensed by pyrene-actin quenching occurs after P_i has dissociated from the protein and likely represents a much larger cleft closure than is seen in our putative P_iR state. A recent attempt to use molecular dynamics simulations to explore a state in which the cleft was forced to close in a Rigor-like manner, while not allowing the lever arm to move, resulted in a structure that did not open the inner cleft, leaving phosphate trapped (Preller and Holmes, 2013). Thus, this simulation did not capture the key features of the P_iR structure.

In this putative P_i release state, a kink of the SH1 helix occurs and is linked to several changes that allow the N-terminal (Nter) subdomain, the relay, and the SH1 helix to interact in such a way as to keep the converter/lever arm primed (Figure S3). The interface between the relay and both the SH1 helix and the converter remains largely the same in the PPS and P_iR states, but a kink of the myosin VI SH1 helix between Val697 and Leu698 allows the formation of new interactions with the Nter subdomain.

Introduction of P_i into the Putative P_i Release Structure

To demonstrate that this structure allows access of phosphate to the active site (i.e., reverse transit of the release), crystals were soaked with 25–100 mM P_i. A series of quick-freezing experiments generated three distinct structures. The most rapid freezing (see Experimental Procedures) gave rise to one of two crystal structures that were unchanged except for the inclusion of P_i. In the first type of crystal, the phosphate was at the exit of the putative P_i release tunnel (referred to as P_iR1 in Table S1), coordinated by S153, T197, S203, R205, and E461 (Figures 4A and 4C; Figure S4A, left panel). In the second type of crystal (P_iR2 in Table S1), the P_i is near ADP (Figure 4A; Figure S4A, middle panel). With delays before freezing, the PPS state was reformed with P_i and MgADP trapped. These structures provide strong evidence for the observed tunnel being able to allow phosphate to transit from solution to the active site and vice versa. Thus, this tunnel can serve as the P_i escape route (Movie S2). It further demonstrates that P_i reentry to the tunnel promotes closure of the back door and isomerization to the PPS state. This has important implications for the interpretation of a number of experiments in muscle fibers and with myosin V_a, as discussed later.

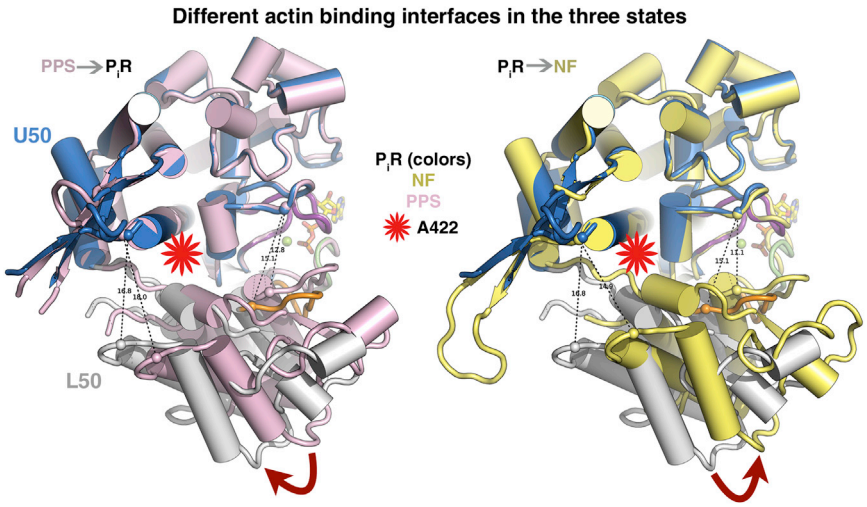

Figure 3. Actin-Binding Elements and Subdomains of Myosin in Different States

The actin-binding interface of myosin, which includes elements of the upper 50 (U50, blue) and L50 (white) subdomains, are presented as viewed from F-actin. Comparison of the P_iR state (U50, blue and L50, gray), PPS (pink) state, and Rigor (NF, yellow) state show that these three states have three very different actin interfaces. The outer cleft near F-actin is closed in a greater extent in the P_iR state than in the PPS state (left). However the closure of the cleft involves a different rotation of the subdomains than those needed to form the Rigor interface (yellow, right). The position of the A422L mutation, which slows cleft closure, is shown with a red star.

See also Figure S3.

As an important control, Post-Rigor crystals (containing MgADP) were also soaked with P_i. No matter how long the crystals were soaked, the P_i was only detected at the end of the tunnel, coordinated by residues S153, T197, R199, S203, and R205 (Figure S4A, right panel).

Assessing the Putative Phosphate-Release Route

Assays of the kinetic cycle of myosin motors on actin (outlined in Figure 1) rely on the existence of probes that report the structural changes. For the release of phosphate, a phosphate-binding protein (P_iBP) is used that changes its fluorescence when phosphate is released into the solution and binds the P_iBP. Thus, its limitation for the present study is that it cannot report on the translocation of P_i from its position in the P_iR2 state described earlier to the P_iR1 state, but only once the P_i is released from P_iR1 binding and moves into the solvent.

To begin to test whether the structure does, in fact, represent the P_i release state induced by actin binding, we made parallel sets of mutations in our putative P_i release tunnel in myosin VI and in myosin V, as well as in DdII. Myosin VI and myosin V have rapid P_i release, while DdII generally has been thought to have slow, rate-limiting P_i release, as do all studied myosin II isoforms. However, at ultra-low ionic strength, fast P_i release has been reported for DdII as well as for skeletal muscle myosin II (Muretta et al., 2013; White et al., 1997). While these low-ionic-strength conditions are not of physiological relevance, the observation does suggest that the formation of the initial interactions with actin is weak and rate limiting rather than P_i release per se. It is particularly important to examine DdII, as its structures have been used to generate proposals of the P_i release mechanism involving a switch I movement (Geeves and Holmes, 2005; Cecchini et al., 2010). Using the low-ionic-strength conditions that allow rapid P_i release also provided the opportunity to observe that the major cleft closure (the so-called weak-to-strong transition) follows P_i release in myosin II, as it does for myosin V and myosin VI (Table 1).

The first mutation, S203A in myosin VI, was designed to slow entry of the P_i into the tunnel (serine 203 in myosin VI plays the role of guiding the P_i away from the active site). We also attempted to impede the exit of P_i from the tunnel by introducing a combination of bulk and repulsive charge (A458E in myosin VI). These two myosin VI mutations correspond to S217A and Y439E in myosin V_a and to S236A and S456E in DdII. A summary of the kinetic results from the mutations, as well as the rationale for each mutation, is given in Table 1.

A structure of the myosin VI P_i release state (P_iR) with the A458E mutation was also obtained. Figure 4 illustrates the P_i tunnel (with P_i in two positions) with these altered residues. The structure of the A458E mutant also reveals that there is sufficient room for the E side chain to assume an alternative, non-blocking position. Thus, we would expect this mutation to slow rather than prevent P_i release, and that the magnitude of the effect may be context (i.e., isoform) dependent. This is consistent with the data shown in Table 1.

The results in Table 1 are all consistent with the P_i release route revealed in the P_iR structure as being the P_i release route used by myosins II, V, and VI when they interact with actin. Previous studies on the S217A mutation in myosin V revealed that it slows hydrolysis as well as P_i release, thus slowing the overall cycling rate (Forgacs et al., 2009). The most convincing mutation is the one that was created to slow P_i moving into the putative channel by a combination of bulk and repulsive charge (A458E, Y439E, and S456E for myosin VI and equivalent residues in myosin V and DdII), which is depicted in Figure 4D). The largest effect was in myosin II at low ionic strength, where P_i release was slowed more than 100-fold, followed by myosin VI with a 3-fold slowing, while myosin V_a showed only a modest slowing of about 20%. We noted that the mutations tended to slow the steady-state actin-activated ATPase (Table 1) of myosin V and myosin VI, which appears to be the result of slowing ADP release from myosin bound to actin in addition to P_i release (myosin VI wild-type [WT] = 6.0 ± 0.1/s; A458E = 1.3 ± 0.1/s; myosin V WT = 17.0 ± 0.5/s; Y439E = 4.0 ± 0.4/s).

The modest effect of the Y439E mutation on P_i release for myosin V may relate to the relatively high affinity of myosin V in its "weak" binding states (Yengo et al., 2002), which could allow it to dwell on actin long enough in the P_i release conformation for a rearrangement of the glutamate side chain position to unblock the P_i release tunnel. To further assess this conjecture, we weakened the binding of myosin V by introducing a

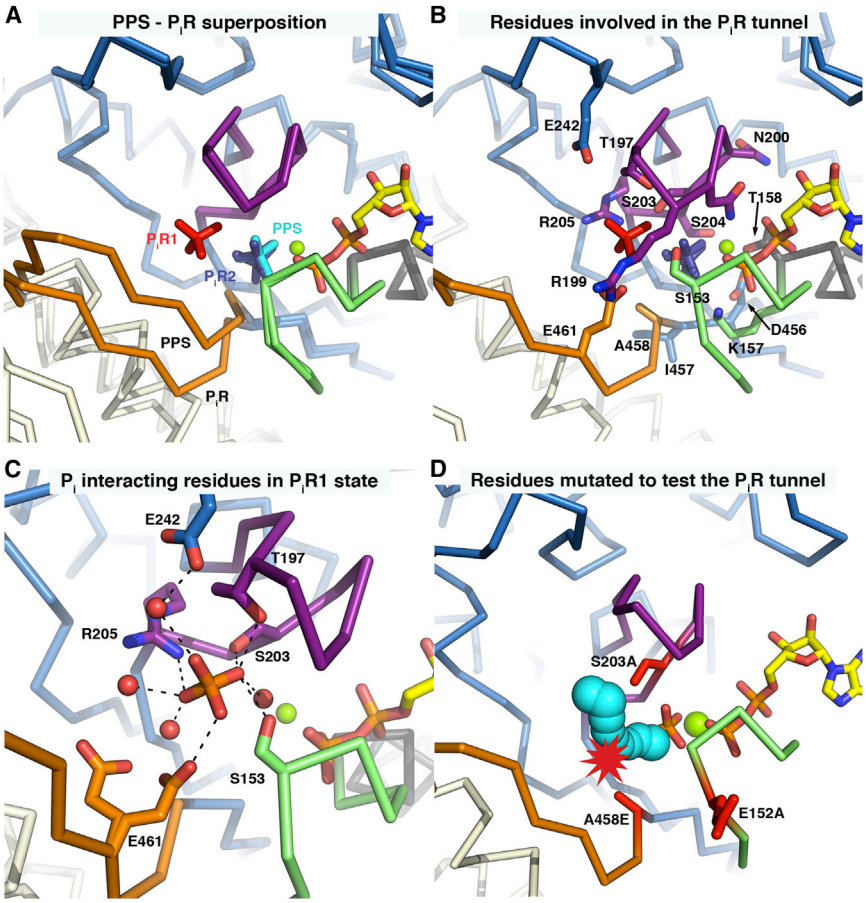

Figure 4. P_i Release Tunnel

Opening of Switch II and Formation of a Tunnel Allowing the Release of P_i.

(A) Superposition of the PPS and the P_iR states showing the opening of switch II (orange) while the conformation of switch I (violet) and the P loop (lime) stay unchanged. The position of the P_i in the structures obtained after P_i soaking is indicated: P_iR1 (red) at the end of the tunnel, P_iR2 (blue) close to ADP, and PPS (cyan; the site in which the P_i is generated upon ATP hydrolysis).

(B) Shown are the side chains of residues in the active site (stick representation); in particular, S203, R205, and E461 define the P_i release pathway in the P_iR state.

(C) Interactions that stabilize the presence of P_i at the end of the putative phosphate-release tunnel (P_iR1 state). The P_i interacts directly with S153, T197, S203, R205, and E461 and via a water molecule with E242.

(D) The residues mutated to test the P_i release tunnel are in red. The S203A was designed to impede P_i entry into the phosphate tunnel seen in PiR; the A458E was designed to add a bulky and charged residue in the tunnel (the red star indicates how this mutation will perturb the Pi pathway, shown in cyan); and E152A was designed to remove a bulky and charged residue from the alternative P_i release pathway (Cecchini et al., 2010).

See also Figure S4 and Table 1.

mutation in the activation loop (K502E, discussed later) and then introduced the Y439E mutation. In this context, the glutamate slowed P_i release approximately 10-fold (Table 1). Note that results with this switch II mutation are not consistent with a switch I/P loop movement occurring to allow P_i release, as previously proposed (Geeves and Holmes, 2005; Cecchini et al., 2010). In this model, P_i release should not be affected by this switch II mutation, since this residue does not impact switch I/P loop movements, and it is positioned far from the proposed alternative P_i exit route.

To further test this alternative P_i release route, we made a mutation (E152A in myosin VI, E164A in myosin V, and E180A in DdII) that had been suggested by molecular dynamics simulations (Cecchini et al., 2010). As discussed earlier, rearrangement of switch I that would maintain MgADP coordination would be necessary if this were the case. This mutation had no effect on P_i release (Table 1), which is consistent with there being no major rearrangement of switch I prior to MgADP release. It is interesting that removal of this glutamate residue slows ADP release (Table 1), which could indicate a role for promoting inner cleft closure necessary for ADP release.

Cleft Closure Must Follow Phosphate Release

The major cleft closure that leads to what has been characterized as strong actin binding is detected in kinetic experiments as a quenching of a pyrene label on actin (De La Cruz et al., 1999). The transition that is sensed is known as the weak-to-strong transition on actin. Since the labeled residue on actin (Cys374) is thought to be outside of the actin-myosin interface, this pyrene signal may indicate that, as the cleft in myosin fully closes and allows a wider interaction surface with the track, the F-actin filament structure is also perturbed. This pyrene-quenching cleft closure precedes the release of MgADP (Sweeney and Houdusse, 2004); thus, the major cleft closure on actin occurs prior to the formation of the Rigor state. To provide strong evidence that this major cleft closure occurs after P_i has been released, we designed mutants that should slow cleft closure by introducing a bulky side chain (leucine) into the myosin outer cleft near the strut and the actin-binding site (A422L, A402L, and A420L for myosin VI, myosin V, and DdII, respectively) (Table 1). This mutation should interfere with formation of the Rigor-like cleft closure but not the rather different cleft closure seen in the P_iR structure (Figure 3; Figure 5). Notably, these mutations did not affect the P_i release rate but greatly slowed the rate of pyrene-actin quenching (weak-to-strong transition), consistent with the major closure at the outer cleft not being necessary for P_i release and occurring subsequent to P_i release, during the transition that may be coupled to lever arm movement (as investigated in experiments described later). It is interesting that the steady-state actin-activated ATPase was slowed to a much greater extent than was the rate of pyrene-actin quenching, suggesting that multiple actin-associated transitions are affected by this cleft mutation.

Table 1. Kinetics of Myosin Constructs: Rates of P_i Release; Cleft Closure, or "Weak-to-Strong" Transition; and Actin-Activated ATPase Activity for Myosin Constructs

Construct Design	Myosin (Mutation)	Phosphate Release (s^{-1})	Cleft Closure (s^{-1})	Steady-State ATPase	
				V_{max} (head^{-1} s^{-1})	K_{ATPase} (μM)
WT motor	Myosin VI	90 ± 6	30 ± 3	6 ± 0.1	3 ± 0.5
	Myosin V_a	143 ± 7	38 ± 4	17 ± 0.5	2 ± 0.4
	Myosin II	103 ± 3[a]	28 ± 4	–	–
Impeding P_i entry into putative phosphate tunnel seen in P_iR structure	Myosin VI (S203A)	43 ± 5	ND	2.4 ± 0.1	9 ± 1.3
	Myosin V_a (S217A)	41 ± 5	ND	5.0 ± 0.3	11 ± 1.6
	Myosin II (S236A)	0.2 ± 0.5[a]	ND	–	–
Bulk and charge in putative phosphate tunnel seen in P_iR structure	Myosin VI (A458E)	29 ± 3	ND	1.3 ± 0.1	2 ± 0.3
	Myosin V_a (Y439E)	117 ± 5	ND	4.0 ± 0.4	1 ± 0.2
	Myosin II (S456E)	0.4 ± 0.2[a]	ND	–	–
Removal of bulk and charge from alternative P_i release pathway (Cecchini et al., 2010)	Myosin VI (E152A)	94 ± 5	20 ± 2	1.0 ± 0.2	4 ± 0.6
	Myosin V_a (E164A)	154 ± 6	23 ± 3	2.7 ± 0.4	3 ± 0.5
	Myosin II (E180A)	101 ± 5[a]	16 ± 3	–	–
Impeding the closure of actin-binding cleft to slow weak-to-strong transition	Myosin VI (A422L)	98 ± 8	6 ± 3	0.15 ± 0.05	15 ± 4
	Myosin V_a (A402L)	140 ± 9	4 ± 1	0.26 ± 0.09	10 ± 2
	Myosin II (A420L)	98 ± 6[a]	9 ± 4	–	–
Reversal of charge in activation loop to slow P_i release state formation	Myosin VI (R521E)	36 ± 5	17 ± 3[b]	4.4 ± 0.3	25 ± 4
	Myosin V_a (K502E)	10 ± 1	8 ± 3[b]	5.1 ± 0.8	15 ± 3
	Myosin II (R520E)	28 ± 6[a]	15 ± 0.5[a,b]	–	–
Activation loop mutation + Bulk and charge in phosphate tunnel	Myosin V_a (K502E + Y439E)	1.1 ± 0.3	ND	0.36 ± 0.1	11 ± 3

Mean values (±SD) of three to five independent protein preparations are shown for each construct and condition. Since P_i release precedes cleft closure, for mutations that result in a marked slowing of phosphate release, an apparent slowing of the subsequent rate (cleft closure) is observed even if the true rate is unchanged. Thus, we only attempted to measure the cleft closure rate in constructs that had a P_i release rate of ~100/s or greater. The one exception was for the mutations in the activation loop. The apparent slowing of cleft closure in those cases was consistent with an unchanged actual rate of cleft closure. ND, not determined.

[a]Low-ionic-strength buffer (0.4 mM $MgCl_2$, 1 mM MOPS, pH = 7.0). Note that the steady-state assay used in this study cannot be performed at this low ionic strength (noted by a dash).

[b]Apparent rate (follows P_i release), consistent with actual rate being ~30 s^{-1}.

Surface Loops Allow Formation of the Phosphate-Release State

Binding to actin is necessary to stabilize this P_i release state, since myosin does not normally release P_i at a high rate in the absence of actin. The docking on actin of the myosin PPS state is initiated by non-stereo-specific, electrostatic interactions. Exploration of the actin surface guided by electrostatic interactions must catalyze the formation of stereospecific actin binding of the P_iR state, promoting release of P_i. From a variety of experimental data, a number of the loops on the myosin surface could create these initial electrostatic interactions with actin (Sasaki et al., 1999; Wang et al., 2000; Joel et al., 2001; Onishi et al., 2006). For this study, we focused on one of the actin-binding loops that has previously been implicated in triggering the initiation of force generation and has been termed the activation loop (Várkuti et al., 2012). This loop is in the L50 subdomain, interacts with the N terminus of actin, and is in a position to help create an interface for our P_iR structure with actin, possibly promoting the L50 subdomain rotation away from its PPS position. We created a mutation that was previously shown (Várkuti et al., 2012) to interfere with force generation in myosin II and myosin V (R520E in DdII and K502E and R521E in myosin V and VI). In all of the myosin classes, this mutation greatly slowed the rate of P_i release (Table 1), consistent with the activation loop playing a role in stabilization of the P_iR state on actin and, thus, in the initiation of force generation. The mutations in this loop did not appear to impact either the actual rate of cleft closure (although the apparent rate was slowed; Table 1) or the rate of ADP release from myosin bound to actin for myosin VI (WT = 6.0 ± 0.1/s versus R521E = 6.3 ± 1.1/s) or myosin V (WT = 17.0 ± 0.5/s versus K502E = 15.9 ± 1.8/s).

DISCUSSION

The P_iR state that we present has all of the hallmarks that are necessary for initiation and optimization of myosin force generation, including creating a different actin-binding interface from that in the PPS state, which allows P_i release to occur before the bulk of the lever arm movement while maintaining high affinity for MgADP. What is revealed by the structure is that, while there is some degree of cleft closure at the outer cleft near actin, this occurs differently from what is necessary for the major cleft

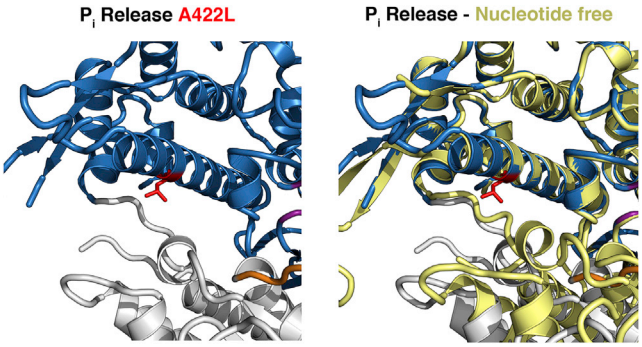

Figure 5. Impairment of Cleft Closure in the Myosin VI A422L Mutant
Note that the mutant side chain of L422 (red), which belongs to the HO helix of the upper 50 (U50) subdomain, does not impair the movement required to populate the P_iR state, in which the closure of the outer cleft is drastically different from that found in Rigor. In contrast, the position of the strut and the L50 subdomain found in the Rigor state (nucleotide-free) drastically differ upon full closure of the cleft. A clash occurs between the L422 side chain and the new position of the strut and slows the transition required to close the cleft.

closure seen in Rigor-like structures (Figure 3). The cleft position has similarities to that found in the Post-Rigor state but is formed by a different switch II movement. The changes at the actin interface in the transition from the PPS to the P_iR state are achieved by a coordinated movement of switch II and the L50 subdomain from their PPS positions. A large shift in switch II position creates an opening for P_i release while having a minimal impact on the lever arm position, which remains in a "primed" position. Note that different switch II positions in the Rigor and Post-Rigor states allow the lever arm to remain in the post-stroke position upon detachment from actin, even though the motor is undergoing major internal rearrangements (Coureux et al., 2003, 2004). Thus, switch II controls lever arm position, but not in a simple two-state manner ("in" and "out") as is often described in the literature (Reubold et al., 2003).

While our structural data are based primarily on myosin VI, which is a reverse-direction myosin (Wells et al., 1999), the reversal of directionality is due to the unusual myosin VI lever arm and not to changes within the motor. When the unusual lever arm is removed or replaced, the core motor of myosin VI is revealed to be a plus-ended motor (Bryant et al., 2007; Park et al., 2007) and undoubtedly shares the common motor mechanism found in all myosin classes. Further support for the generality of this P_iR state comes from our demonstrating that DdII can also form this state (Figure S2B) and from the fact that mutations in class VI, V, and II myosins have a similar impact on P_i release.

The emerging view is that myosin is initially bound to actin via electrostatic interactions with loop 2 and likely other flexible surface loops, such as the HCM loop (Onishi et al., 2006; Sasaki et al., 1999; Wang et al., 2000; Liu et al., 2005). Once these loops orient the myosin PPS state on actin, presumably mostly via electrostatic interactions (given the acceleration of P_i release from myosin II at extremely low ionic strength), actin can trigger P_i release by inducing the transition to the more strongly and stereo-specifically bound P_iR state. Formation of the stereo-specific binding interface involves hydrophobic residues, including the actin-binding region (helix-loop-helix) in the L50 subdomain (Kojima et al., 2001; Sasaki et al., 2002), which may initially be positioned by the activation loop. This loop indeed plays an important role for promoting the transition that populates the P_i release state on actin and thus accelerates release of P_i (Table 1; Várkuti et al., 2012). What the P_iR structure reveals is that the sequential myosin-actin interactions during the powerstroke promote different states of the motor that are initiated and gated by the control of P_i release. P_i release must occur only upon stereo-specific binding to actin and must trigger subsequent rearrangements that control force production and lever arm movement.

In comparing myosin V_a, which releases P_i rapidly on actin, to myosin II, which releases P_i slowly except at extremely low ionic strength, it has been shown that the weak interactions with actin in the PPS state are stronger in the case of myosin V_a (Yengo et al., 2002). This is consistent with the assertion that the loop interactions are critical for stabilizing the binding of the PPS state that promotes the subsequent transition to the P_iR state, triggering P_i release. While the general features of the P_iR state are likely conserved within the family, how much of the tuning of the rates occurs via the actin-binding loops or the internal sequence of the motor remains to be studied and will elucidate how the cellular motors are perfectly suited to their precise action. It is interesting that P_i release is the step affected for the deafness R156W mutation in Myo1c (Lin et al., 2011). Structural insights can now explain how this mutation affects the duty ratio, since the tryptophan side chain slows down the opening of the back door.

As illustrated in (Figure 6), force production would begin when a myosin head attached to actin in the PPS state via ionic interactions transitions to the P_iR state, which then binds in the first stereo-specific, force-bearing state on actin. The P_iR state is likely equivalent to the state first described by Sleep and Hutton (1980), in which force production is initiated and P_i rebinding is possible (Caremani et al., 2008). In the absence of strain, P_i release is virtually irreversible due to the next structural transition involving cleft closure coupled to lever arm movement. In this scheme, the difference between a myosin that releases P_i slowly on actin, such as DdII, and a myosin that releases P_i rapidly, such as myosin V_a or myosin VI, is based on the affinity that these myosin loops mediate for F-actin as well as their influence on the equilibrium between the PPS state and P_iR state when the myosin is bound to actin. Thus, variability in the nature of the myosin surface loops strongly influences the rate of entry into the force-generating states.

Creation of a Strong Binding Actin Interface

While the pyrene probe at Cys374 on actin has been used to monitor the so-called weak-to-strong transition on actin, we propose that it reports on the major cleft closure but not the initial formation of a strong actin-binding state, which would be the beginning of force generation. We propose that the initial closure of the outer cleft and strong binding to actin occurs upon formation of the P_iR state. This initial strong binding state forms with minimal movement of the lever arm. The major movement of the lever arm (powerstroke) is coupled to the further cleft closure following P_i release and presumably cannot occur until P_i moves away from the active site. In this regard, P_i at the active site may act as a wedge to prevent Rigor-like cleft closure. This

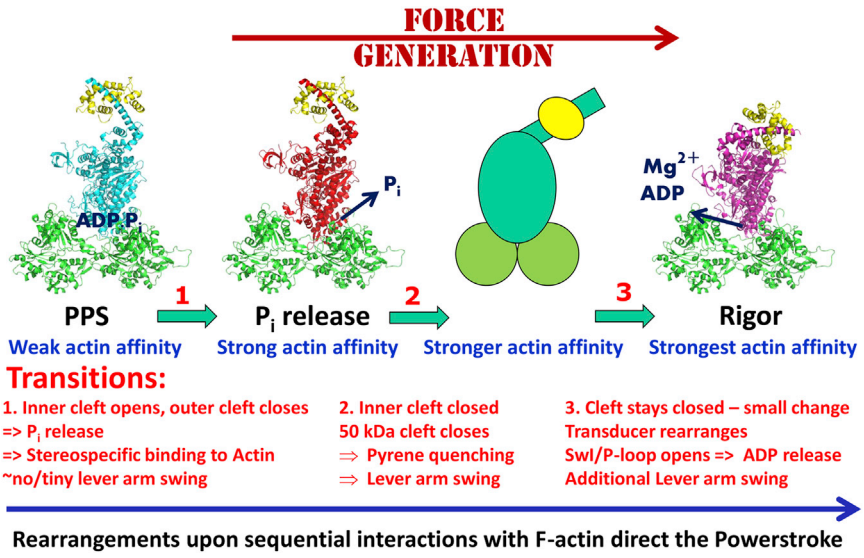

Figure 6. Model for Myosin Force Generation

Shown are the structural transitions that underlie chemo-mechanical transduction by myosin. With the description of the P_iR state, herein, only the structural changes associated with the strong ADP-binding, actin-bound state remain to be elucidated.

mechanism would also prevent the Post-Rigor myosin.MgATP state from reforming a strong actin interface due to the presence of the gamma-phosphate in the active site. Note that the myosin.MgADP Post-Rigor state can readily undergo the weak-to-strong transition on actin.

It is also clear that once P_i is released and the weak-to-strong transition occurs, the resulting myosin.MgADP complex affinity for actin is not as high as the Rigor-binding affinity (De La Cruz et al., 1999), suggesting that until the MgADP coordination is broken and the active site is completely open (Coureux et al., 2004), the cleft cannot completely close. Thus, a model emerges of at least three distinct types of cleft closure associated with strong binding to actin: the one seen in the P_iR state, the one yet to be seen at high resolution in the strong MgADP-binding state, and the one that has been shown for Rigor (Coureux et al., 2003). In order to drive the cycle forward, the affinity of each of these states for actin should increase, beginning with P_i release and ending with Rigor.

A key remaining question is what is the actin affinity of the P_iR state. Since none of our mutations trapped this state, we had no way to directly measure its actin-binding affinity. Earlier results with myosin V_a trapped in the Post-Rigor ATP state allowed determination of an actin affinity of ~2 μM. Surprisingly, adding AMPPNP resulted in a much higher actin affinity (~0.3 μM) without formation of a pyrene-actin quenching interface (Yengo et al., 2002). These affinities are much higher than that of the myosin V_a PPS state for actin, which was estimated at >10 μM (De La Cruz et al., 1999). Given our new findings, it is possible that myosin V_a.AMPPNP binds to actin with an interface that is similar to our P_iR state. This is consistent with our current hypothesis that P_i in the active site prevents Rigor-like cleft closure but allows binding to actin with the P_iR interface. In further support of this speculation, electron microscopy reconstructions of myosin V_a bound to actin in the presence of AMPPNP displayed a lever arm in a primed position (Volkmann et al., 2005). Thus, the affinity of the P_iR state for actin may be much higher than that of the weak binding state, PPS, as would be expected if it is the first state in force generation on actin.

The three distinct cleft conformations described earlier are likely coupled to distinct positions of the myosin lever arm. To optimize force generation, only a small lever arm movement should occur prior to strong binding of actin in the state necessary to initiate P_i release. The remainder of the powerstroke would then occur in at least two discrete movements in the absence of load. A large movement would be expected to accompany the major cleft closure at the actin interface (i.e., the pyrene-actin quenching transition), and there is a well-documented second swing upon the release of MgADP (Whittaker et al., 1995; Veigel et al., 2002). Our P_iR structure has a slight repositioning of the myosin lever arm as compared to the PPS structure. The magnitude of this movement may vary among myosin isoforms, given that there is variability in the positioning of the lever arm in the PPS state (Houdusse et al., 2000; Kollmar et al., 2002; Münnich et al., 2014), but in all cases, the bulk of the powerstroke should follow formation of the P_iR state.

The general concept of the lever arm swing following P_i release fits well with single-molecule studies of either skeletal muscle myosin II (Takagi et al., 2006) or myosin V_a (Sellers and Veigel, 2010) undergoing rapid feedback to counter movement. These experiments suggest that the P_i release step is only reversible when the lever arm swing is prevented. Furthermore, kinetic studies of dimeric myosin V demonstrated that P_i is released from the lead head of a dimer at essentially the unstrained rate, while MgADP release from the lead head is greatly slowed (Rosenfeld and Sweeney, 2004). Last, muscle fiber studies suggest that the P_i release step is only reversible if the myosin lever arms are at a position near the beginning of the powerstroke (Dantzig et al., 1992; Caremani et al., 2008). All of these results support the concept that the major component of the powerstroke follows P_i release.

Initiation of Lever Arm Movement

We postulate that P_i occupancy of the nucleotide pocket near the MgADP (P_iR2 in Figures 4A and S4A and Table S1) prevents full cleft closure and the lever arm movement associated with the powerstroke. We further postulate that once the P_iR2 state forms on actin, the P_i can rapidly translocate through the phosphate tunnel and occupy the position at the mouth of the P_i release tunnel, as seen in the structure referred to as P_iR1 in Figure 4A and Table S1. Once in this position, it is likely that the motor can begin to close the cleft to form a stronger interface with actin with a concomitant movement of the lever arm (i.e., the beginning of the powerstroke). This would make the P_i release

essentially irreversible in the absence of load. As discussed earlier, if the lever arm is prevented from moving, then the P_i release tunnel would remain open, allowing P_i to return to the active site.

Note that our P_i release assay only detects the P_i once it is in solution, having left its position at the mouth of the release tunnel. If the structural rearrangements that begin to close the actin cleft and move the lever arm are more rapid than the movement of P_i from its position in the P_iR1 state, then it could appear that lever arm movement and cleft closure precede P_i release, but this would simply reflect the limitations of our assays. There is a report (Muretta et al., 2013) that suggests that P_i is released after the major lever arm movement. While the authors interpret this as evidence for a lever arm swing gating P_i release, we argue that it may simply reflect that it is the movement of P_i from its P_iR2 position to its P_iR1 position in the P_iR state that gates lever arm movement but that this is not directly detected by the phosphate-release protein assay, which only senses the P_i once it is in solution. Since the lever arm swing that Muretta et al. detected is likely accompanied by cleft closure, but is much faster than the weak-to-strong transition on actin, it is unclear whether the pyrene actin detects a further closure of the cleft accompanied by additional movement of the lever arm or whether it could represent a rearrangement of the actin that follows myosin cleft closure, which allows an even stronger actin-myosin interface to form. Clarification of these points will require additional kinetic probes of myosin structural rearrangements.

Note that our model based on the structural and kinetic data in this paper differs significantly from a recent molecular dynamics simulation of the beginning of the powerstroke (Preller and Holmes, 2013). In this simulation, the cleft near actin was forced into a Rigor-like interface, the lever arm remained close to the primed position seen in PPS, and both P_i and MgADP remained trapped at the active site. We demonstrate, in fact, that an actin interface much different from the Rigor interface must first form to allow the departure of P_i from the active site and that, subsequent to this event, further cleft closure coupled to lever arm movement occurs, promoting formation of the Rigor actin-binding interface. Thus, in our model, P_i translocation away from the active site gates the cleft closure that is coupled to the major movement of the lever arm, which is known as the powerstroke.

Conclusions

Our study highlights a mechanism for opening the escape route for P_i that might also be used for other cellular machines powered by ATP and GTP. It differs from the mechanism supported by studies of motors such as F1ATPase (Menz et al., 2001), in which a rearrangement of the central beta sheet must occur. Lessons from myosin could shed light on models for dynamins or ATPases, such as FlaI (Reindl et al., 2013), in which binding to partners gates and precedes force production.

Given all of the data, we assert that the structural state of myosin that we present in this paper is, in fact, the P_i release state, the first actin-bound state in force generation. This study provides insights into how force production is controlled and tuned in the myosin superfamily. Visualizing this structure is necessary for understanding how myosin motors choose their cellular track and how they perform such different cellular actions. It provides essential information to account for the effect of numerous mutations that have been reported in human genetic disorders in more than 12 myosin classes, including cardiomyopathy (cardiac myosin) and microvillus disease (myosin 5b). This structure also provides a framework to rationally design drugs that can slow, block, or accelerate force production in myosins that have been mis-tuned by disease-causing mutation.

EXPERIMENTAL PROCEDURES

Expression Constructs, Production, and Purification

Recombinant DNA of porcine myosin VI, chicken myosin V_a, or DdII were generated to express various truncated myosin constructs containing the motor domain of these myosins using the baculovirus expression system. For the P_i release myosin VI crystal structures, a C-terminal truncation was made at I789, creating the MD construct. This truncation is at the end of the first (proximal) helix of insert 2 and precedes the CaM-binding site of insert 2. All the kinetic studies described with myosin VI were performed from WT or point mutation introduced in the construct MD^{ins2} truncated at the end of insert 2, after residue A816, prior to the CaM-binding IQ motif. For the soaking of Post-Rigor crystals, the construct $MD^{ins2\text{-}delta.ins1}$ was used, since it crystallizes in this state. In this MD^{ins2} construct, insert 1 (residues C278–A303) was removed as previously described (Ménétrey et al., 2005, 2008). Each of these three constructs (MD, MD^{ins2}, and $MD^{ins2\text{-}delta.ins1}$) had a Flag tag (encoding DYKDDDDK) appended via a glycine to the N terminus to facilitate purification. For the *Dictyostelium* MD, the DNA corresponds to the construct truncated after the codon corresponding to R761 with a C-terminal flag. All kinetic studies described for myosin V_a were performed from WT or point mutation introduced in the chicken myosin V_a construct (MD1IQ) truncated after the codon corresponding to R792 with a C-terminal flag, as previously studied (De La Cruz et al., 1999). This construct encompassed the motor domain and the first light chain/calmodulin-binding site of myosin V_a. The myosin V_a-expressing virus was co-infected with a virus encoding a truncated human essential light chain (LC-1sa) (De La Cruz et al., 2000) as previously described (Coureux et al., 2003). These constructs were used to create recombinant baculoviruses for expression in SF9 cells as previously described (De La Cruz et al., 1999). All of the expressed myosin molecules were purified as previously described (Sweeney et al., 1998).

Crystallization and Data Collection

Crystals of myosin VI in the P_iR state were obtained with the MD construct using the hanging-drop vapor-diffusion method. Spontaneous nucleation occurred at 277 K with equal amounts of reservoir solution (containing 6.25% polyethylene glycol [PEG] 8000, 50 mM TRIS, pH 8.5, 1 mM TCEP, 3% glycerol) and stock solution of the protein (10 mg/ml^{-1} in 10 mM HEPES, pH 7.5, 50 mM NaCl, 1 mM TCEP, 1 mM NaN_3 with 2 mM Mg^{2+}ADP). The best crystals were obtained using seeding approaches. Further details of the experiments performed for this study are indicated in the Supplemental Experimental Procedures. Crystals of proteins were obtained and were cryo-cooled prior to data collection at either the European Synchrotron Radiation Facility (ESRF) or SOLEIL Synchrotron beamlines. The data sets were processed with XDS (Kabsch, 2010). Statistics on the data collection for five new P_i release myosin VI structures, one Post-Rigor structure frozen after long P_i soaking, one PPS myosin VI structure obtained after long P_i soaking of a P_iR myosin VI crystal, and a *Dictyostelium* R238E, E459R myosin II structure are indicated in Table S1. Statistics of the final models are also summarized in Table S1. Details of structure determination, model building, and refinement are indicated in the Supplemental Experimental Procedures.

Kinetic Experiments

For the transient kinetic experiments, which are essentially single-turnover experiments, the general strategy can be summarized as follows. For the measurement of P_i release, P_i that is released from myosin is detected by binding to a phosphate-binding protein that is labeled so that a change in fluorescence is observed upon P_i binding (White et al., 1997). Turnover is inhibited after the initial transient by including MgADP in the final mix. Cleft closure is detected by the quenching of a pyrene label on actin. However, this rate can only be accurately measured if phosphate release—which, as demonstrated in this study,

precedes cleft closure—is much faster than cleft closure as it is in WT myosin V and myosin VI. Again, turnover is inhibited after the initial transient by including MgADP in the final mix. In general, we only attempted this measurement for constructs that displayed a P_i release rate of 100/s or greater. The exception was for mutations in the activation loop (Table 1), which greatly slowed P_i release and the apparent rate of cleft closure, but the calculated rate of cleft closure (assuming that the observed rate is limited by both P_i release and cleft closure) is similar to the WT rate. The rate of ADP release from the actin-myosin complex was measured for a subset of constructs by binding mantADP to the myosin, then competing it off with unlabeled ADP and measuring the rate of fluorescence decrease as the mant signal was quenched by exposure to solvent.

ACCESSION NUMBERS

The atomic coordinates and structure factors of eight structures have been deposited in the Protein Data Bank (www.pdb.org) with accession numbers PDB: 4PFO (P_iR), 4PFP (P_iR-P21), 4PJN (P_iR1), 4PJM (P_iR2), 4PK4 (PPS-0), 4PJJ (PR-P_i), 4PJL (P_iR-A458E), and 4PJK (Dy-R238E.E459R-P_iR) (Table S1).

SUPPLEMENTAL INFORMATION

Supplemental Information includes Supplemental Experimental Procedures, four figures, one table, and two movies and can be found with this article online at http://dx.doi.org/10.1016/j.devcel.2015.03.025.

AUTHOR CONTRIBUTIONS

P.L., T.I., and L.S. contributed equally to this work. P.L. and T.I. determined the structures and analyzed them with A.H. Biochemical experiments were performed by V.R., H.B., S.S., and C.K.; C.M., L.S., and B.Z performed kinetic studies. A.H. and H.L.S. conceived the project, oversaw the experiments, analyzed them, and wrote the manuscript.

ACKNOWLEDGMENTS

We thank Xiaoyan Liu for the expression and purification of the protein for structural studies. We thank Pierre Legrand and Andy Thompson as well as beamline scientists of PX1 (SOLEIL Synchrotron), ID23-2, and ID29 (ESRF Synchrotron) for excellent support during data collection. A.H. was supported by grants from the CNRS, Équipes FRM, ANR 2010 BLAN 1504 01 and ANR-13-BSV8-0019-01, Ligue Contre le Cancer, and ARC subvention fixe. H.L.S. was supported by NIH grants DC009100 and HL110869. The A.H. team is part of Labex CelTisPhyBio 11-LBX-0038, which is part of the IDEX PSL (ANR-10-IDEX-0001-02 PSL).

Received: August 3, 2014
Revised: February 23, 2015
Accepted: March 30, 2015
Published: April 30, 2015

REFERENCES

Bryant, Z., Altman, D., and Spudich, J.A. (2007). The power stroke of myosin VI and the basis of reverse directionality. Proc. Natl. Acad. Sci. USA *104*, 772–777.

Caremani, M., Dantzig, J., Goldman, Y.E., Lombardi, V., and Linari, M. (2008). Effect of inorganic phosphate on the force and number of myosin cross-bridges during the isometric contraction of permeabilized muscle fibers from rabbit psoas. Biophys. J. *95*, 5798–5808.

Cecchini, M., Alexeev, Y., and Karplus, M. (2010). Pi release from myosin: a simulation analysis of possible pathways. Structure *18*, 458–470.

Coureux, P.-D., Wells, A.L., Ménétrey, J., Yengo, C.M., Morris, C.A., Sweeney, H.L., and Houdusse, A. (2003). A structural state of the myosin V motor without bound nucleotide. Nature *425*, 419–423.

Coureux, P.-D., Sweeney, H.L., and Houdusse, A. (2004). Three myosin V structures delineate essential features of chemo-mechanical transduction. EMBO J. *23*, 4527–4537.

Dantzig, J.A., Goldman, Y.E., Millar, N.C., Lacktis, J., and Homsher, E. (1992). Reversal of the cross-bridge force-generating transition by photogeneration of phosphate in rabbit psoas muscle fibres. J. Physiol. *451*, 247–278.

De La Cruz, E.M., Wells, A.L., Rosenfeld, S.S., Ostap, E.M., and Sweeney, H.L. (1999). The kinetic mechanism of myosin V. Proc. Natl. Acad. Sci. USA *96*, 13726–13731.

De La Cruz, E.M., Wells, A.L., Sweeney, H.L., and Ostap, E.M. (2000). Actin and light chain isoform dependence of myosin V kinetics. Biochemistry *39*, 14196–14202.

Forgacs, E., Sakamoto, T., Cartwright, S., Belknap, B., Kovács, M., Tóth, J., Webb, M.R., Sellers, J.R., and White, H.D. (2009). Switch 1 mutation S217A converts myosin V into a low duty ratio motor. J. Biol. Chem. *284*, 2138–2149.

Franker, M.A., and Hoogenraad, C.C. (2013). Microtubule-based transport - basic mechanisms, traffic rules and role in neurological pathogenesis. J. Cell Sci. *126*, 2319–2329.

Geeves, M.A., and Holmes, K.C. (2005). The molecular mechanism of muscle contraction. Adv. Protein Chem. *71*, 161–193.

Gyimesi, M., Kintses, B., Bodor, A., Perczel, A., Fischer, S., Bagshaw, C.R., and Málnási-Csizmadia, A. (2008). The mechanism of the reverse recovery step, phosphate release, and actin activation of Dictyostelium myosin II. J. Biol. Chem. *283*, 8153–8163.

Hartman, M.A., Finan, D., Sivaramakrishnan, S., and Spudich, J.A. (2011). Principles of unconventional myosin function and targeting. Annu. Rev. Cell Dev. Biol. *27*, 133–155.

Hirokawa, N., Noda, Y., Tanaka, Y., and Niwa, S. (2009). Kinesin superfamily motor proteins and intracellular transport. Nat. Rev. Mol. Cell Biol. *10*, 682–696.

Houdusse, A., Szent-Gyorgyi, A.G., and Cohen, C. (2000). Three conformational states of scallop myosin S1. Proc. Natl. Acad. Sci. USA *97*, 11238–11243.

Joel, P.B., Trybus, K.M., and Sweeney, H.L. (2001). Two conserved lysines at the 50/20-kDa junction of myosin are necessary for triggering actin activation. J. Biol. Chem. *276*, 2998–3003.

Kabsch, W. (2010). XDS. Acta Crystallogr. D Biol. Crystallogr. *66*, 125–132.

Kojima, S., Konishi, K., Katoh, K., Fujiwara, K., Martinez, H.M., Morales, M.F., and Onishi, H. (2001). Functional roles of ionic and hydrophobic surface loops in smooth muscle myosin: their interactions with actin. Biochemistry *40*, 657–664.

Kollmar, M., Dürrwang, U., Kliche, W., Manstein, D.J., and Kull, F.J. (2002). Crystal structure of the motor domain of a class-I myosin. EMBO J. *21*, 2517–2525.

Kull, F.J., and Endow, S.A. (2013). Force generation by kinesin and myosin cytoskeletal motor proteins. J. Cell Sci. *126*, 9–19.

Lin, T., Greenberg, M.J., Moore, J.R., and Ostap, E.M. (2011). A hearing loss-associated myo1c mutation (R156W) decreases the myosin duty ratio and force sensitivity. Biochemistry *50*, 1831–1838.

Liu, X., Shu, S., Kovács, M., and Korn, E.D. (2005). Biological, biochemical, and kinetic effects of mutations of the cardiomyopathy loop of Dictyostelium myosin II: importance of ALA400. J. Biol. Chem. *280*, 26974–26983.

Ménétrey, J., Bahloul, A., Wells, A.L., Yengo, C.M., Morris, C.A., Sweeney, H.L., and Houdusse, A. (2005). The structure of the myosin VI motor reveals the mechanism of directionality reversal. Nature *435*, 779–785.

Ménétrey, J., Llinas, P., Cicolari, J., Squires, G., Liu, X., Li, A., Sweeney, H.L., and Houdusse, A. (2008). The post-rigor structure of myosin VI and implications for the recovery stroke. EMBO J. *27*, 244–252.

Menz, R.I., Walker, J.E., and Leslie, A.G. (2001). Structure of bovine mitochondrial F(1)-ATPase with nucleotide bound to all three catalytic sites: implications for the mechanism of rotary catalysis. Cell *106*, 331–341.

Münnich, S., Taft, M.H., and Manstein, D.J. (2014). Crystal structure of human myosin 1c—the motor in GLUT4 exocytosis: implications for Ca2+ regulation and 14-3-3 binding. J. Mol. Biol. *426*, 2070–2081.

Muretta, J.M., Petersen, K.J., and Thomas, D.D. (2013). Direct real-time detection of the actin-activated power stroke within the myosin catalytic domain. Proc. Natl. Acad. Sci. USA *110*, 7211–7216.

Onishi, H., Mikhailenko, S.V., and Morales, M.F. (2006). Toward understanding actin activation of myosin ATPase: the role of myosin surface loops. Proc. Natl. Acad. Sci. USA *103*, 6136–6141.

Park, H., Li, A., Chen, L.Q., Houdusse, A., Selvin, P.R., and Sweeney, H.L. (2007). The unique insert at the end of the myosin VI motor is the sole determinant of directionality. Proc. Natl. Acad. Sci. USA *104*, 778–783.

Preller, M., and Holmes, K.C. (2013). The myosin start-of-power stroke state and how actin binding drives the power stroke. Cytoskeleton (Hoboken) *70*, 651–660.

Rayment, I., Rypniewski, W.R., Schmidt-Bäse, K., Smith, R., Tomchick, D.R., Benning, M.M., Winkelmann, D.A., Wesenberg, G., and Holden, H.M. (1993). Three-dimensional structure of myosin subfragment-1: a molecular motor. Science *261*, 50–58.

Reindl, S., Ghosh, A., Williams, G.J., Lassak, K., Neiner, T., Henche, A.L., Albers, S.V., and Tainer, J.A. (2013). Insights into FlaI functions in archaeal motor assembly and motility from structures, conformations, and genetics. Mol. Cell *49*, 1069–1082.

Reubold, T.F., Eschenburg, S., Becker, A., Kull, F.J., and Manstein, D.J. (2003). A structural model for actin-induced nucleotide release in myosin. Nat. Struct. Biol. *10*, 826–830.

Roberts, A.J., Kon, T., Knight, P.J., Sutoh, K., and Burgess, S.A. (2013). Functions and mechanics of dynein motor proteins. Nat. Rev. Mol. Cell Biol. *14*, 713–726.

Rosenfeld, S.S., and Sweeney, H.L. (2004). A model of myosin V processivity. J. Biol. Chem. *279*, 40100–40111.

Sasaki, N., Asukagawa, H., Yasuda, R., Hiratsuka, T., and Sutoh, K. (1999). Deletion of the myopathy loop of *Dictyostelium* myosin II and its impact on motor functions. J. Biol. Chem. *274*, 37840–37844.

Sasaki, N., Ohkura, R., and Sutoh, K. (2002). *Dictyostelium* myosin II as a model to study the actin-myosin interactions during force generation. J. Muscle Res. Cell Motil. *23*, 697–702.

Sellers, J.R., and Veigel, C. (2010). Direct observation of the myosin-Va power stroke and its reversal. Nat. Struct. Mol. Biol. *17*, 590–595.

Sleep, J.A., and Hutton, R.L. (1980). Exchange between inorganic phosphate and adenosine 5′-triphosphate in the medium by actomyosin subfragment 1. Biochemistry *19*, 1276–1283.

Sweeney, H.L., and Houdusse, A. (2004). The motor mechanism of myosin V: insights for muscle contraction. Philos. Trans. R. Soc. Lond. B Biol. Sci. *359*, 1829–1841.

Sweeney, H.L., and Houdusse, A. (2010). Structural and functional insights into the Myosin motor mechanism. Annu. Rev. Biophys. *39*, 539–557.

Sweeney, H.L., Rosenfeld, S.S., Brown, F., Faust, L., Smith, J., Xing, J., Stein, L.A., and Sellers, J.R. (1998). Kinetic tuning of myosin via a flexible loop adjacent to the nucleotide binding pocket. J. Biol. Chem. *273*, 6262–6270.

Takagi, Y., Homsher, E.E., Goldman, Y.E., and Shuman, H. (2006). Force generation in single conventional actomyosin complexes under high dynamic load. Biophys. J. *90*, 1295–1307.

Várkuti, B.H., Yang, Z., Kintses, B., Erdélyi, P., Bárdos-Nagy, I., Kovács, A.L., Hári, P., Kellermayer, M., Vellai, T., and Málnási-Csizmadia, A. (2012). A novel actin binding site of myosin required for effective muscle contraction. Nat. Struct. Mol. Biol. *19*, 299–306.

Veigel, C., Wang, F., Bartoo, M.L., Sellers, J.R., and Molloy, J.E. (2002). The gated gait of the processive molecular motor, myosin V. Nat. Cell Biol. *4*, 59–65.

Volkmann, N., Liu, H., Hazelwood, L., Krementsova, E.B., Lowey, S., Trybus, K.M., and Hanein, D. (2005). The structural basis of myosin V processive movement as revealed by electron cryomicroscopy. Mol. Cell *19*, 595–605.

Wang, F., Harvey, E.V., Conti, M.A., Wei, D., and Sellers, J.R. (2000). A conserved negatively charged amino acid modulates function in human nonmuscle myosin IIA. Biochemistry *39*, 5555–5560.

Wells, A.L., Lin, A.W., Chen, L.Q., Safer, D., Cain, S.M., Hasson, T., Carragher, B.O., Milligan, R.A., and Sweeney, H.L. (1999). Myosin VI is an actin-based motor that moves backwards. Nature *401*, 505–508.

White, H.D., Belknap, B., and Webb, M.R. (1997). Kinetics of nucleoside triphosphate cleavage and phosphate release steps by associated rabbit skeletal actomyosin, measured using a novel fluorescent probe for phosphate. Biochemistry *36*, 11828–11836.

Whittaker, M., Wilson-Kubalek, E.M., Smith, J.E., Faust, L., Milligan, R.A., and Sweeney, H.L. (1995). A 35-A movement of smooth muscle myosin on ADP release. Nature *378*, 748–751.

Yengo, C.M., De la Cruz, E.M., Safer, D., Ostap, E.M., and Sweeney, H.L. (2002). Kinetic characterization of the weak binding states of myosin V. Biochemistry *41*, 8508–8517.

Yount, R.G., Lawson, D., and Rayment, I. (1995). Is myosin a "back door" enzyme? Biophys. J. *68* (4, Suppl), 44S–47S, discussion 47S–49S.